INTERNATIONAL JOURNAL OF AUTOMOTIVE AND MECHANICAL ENGINEERING
ISSN: 2229-8649 e-ISSN: 2180-1606
VOL. 21, ISSUE 4, 2024, 11723 – 11743
DOI: https://doi.org/10.15282/ijame.21.4.2024.1.0904

RESEARCH ARTICLE

Model Reference Adaptive Control of an Independent Steer-by-Wire System: A Simulation Using a 14-Degree-of-Freedom Vehicle Model

M.H. Hamdi[1], F. Ahmad[1]*, M.H.Che Hasan[2], M.H. Harun[1] and V.R. Aparow[3]

[1]Faculty of Mechanical Technology and Engineering, Universiti Teknikal Malaysia Melaka, 75450 Melaka, Malaysia
[2]Faculty of Electrical Technology and Engineering, Universiti Teknikal Malaysia Melaka, 75450 Melaka, Malaysia
[3]Faculty of Science and Engineering, University of Nottingham Malaysia Campus, Jalan Broga, Semenyih, Selangor Darul Ehsan, Malaysia

ABSTRACT – This research delves into how Model Reference Adaptive Control (MRAC) can be applied in an independent Steer-by-Wire (SBW) system, utilising a detailed 14 Degrees of Freedom (DOF) full-vehicle model. This study is all about pushing forward vehicle dynamics and control using SBW technology. This study also has come up with some cutting-edge control algorithms that allow each wheel to be steered independently, which seriously boosts how manoeuvrable and responsive the vehicle is. Through simulations, the study shows that MRAC is a big improvement over traditional control methods where quantitative analysis shows that MRAC reduces yaw rate errors by up to 66.67% compared to Proportional-Integral-Derivative (PID) and 50% compared to Multi-order PID (MOPID). Additionally, in lateral acceleration and sideslip angle controls, MRAC demonstrates a similar reduction in errors, significantly outperforming PID and MOPID with errors maintained well below 10%, proving its worth in predictive control and real-time adaptability to various road conditions and driver intentions. The key finding from this study is that MRAC greatly enhances manoeuvrability and responsiveness compared to standard methods which offer flexibility according to the different driving scenarios. There are notable advancements in vehicle steering systems, which contribute to safer and more efficient driving. In essence, this work marks a significant step forward in automotive steering technology, opening the door to safer and more efficient modern vehicles.

ARTICLE HISTORY
Received : 14th May 2024
Revised : 16th Aug. 2024
Accepted : 28th Aug. 2024
Published : 15th Nov. 2024

KEYWORDS
MRAC controller
Steer-by-wire system
Independent arm
14 DOF vehicle model
Simulation

1. INTRODUCTION

The evolution of vehicle steering systems from traditional rack-and-pinion to advanced Steer-By-Wire (SBW) technology marks a significant advancement in automotive engineering. Traditionally, rack-and-pinion has been indispensable in automotive design, analogous to a fundamental ingredient in the recipe, providing a simple, effective, and intuitive linkage between the steering wheel and the vehicle's wheels, thereby ensuring precise control [1]. However, it is challenged by limitations such as inter-tooth clearance in its mechanism, which can compromise the accuracy and precision of the vehicle's handling, particularly impacting machine tool positioning during setup [2]. Furthermore, considerations such as weight, structural stress, and vibrational dynamics are critical in designing these systems, especially for all-terrain vehicles, to ensure optimal performance and longevity [3]. Contrastingly, SBW technology represents a transformative approach by eliminating mechanical linkages in favour of electronic controls, which interpret the driver's input through sensors and actuators. This innovation not only promises enhanced steering precision and vehicle dynamics but also integrates seamlessly with autonomous driving technologies, laying a foundation for future automotive advancements [4]-[7]. SBW systems offer significant benefits, including improved control and safety, especially critical during emergency manoeuvres where traditional systems' slow response times could be detrimental [8]. Moreover, the removal of mechanical constraints allows for reduced vehicle weight, increased design flexibility, and better energy efficiency, attributes that are especially beneficial in the design of electric vehicles. This transition to SBW enables manufacturers to explore new vehicle designs, fostering greater innovation and safety in automotive development. Despite these advancements, SBW technology is not without its challenges, including issues related to reliability and fault tolerance, as well as the need for advanced motor drives [9,10]. Acknowledging these limitations, the most recent studies have explored further innovations such as the Independent Steer-By-Wire (ISBW) system, which aims to address these specific challenges and push the boundaries of what is possible in vehicle steering technology.

Recent advancements in ISBW technology have been explored by studies such as [11]; the authors summarised and discussed the developments, challenges, and advancements made by various commercial and academic entities on Four-Wheel Independent Drive/Steering Electric Vehicles (4WID-4WIS EVs). As examples, referring from their valuable information, they stated that the concept of four-wheel-independent steering and 4 Wheel-Independent Steering/ 4 Wheel-Independent Driving (4WIS4WID) was notably advanced by industry pioneers such as Toyota and Nissan, with their innovative designs like the Toyota Fine-T followed by the Nissan Pivo series. These vehicles employ a system where each wheel is controlled by its own motor for both steering and driving, enhancing manoeuvrability with capabilities such as lateral movement and zero-radius turns. Despite these advancements, a significant limitation of the 4WIS4WID setup

*CORRESPONDING AUTHOR | F. Ahmad | ✉ fauzi.ahmad@utem.edu.my

is that the orientation of each wheel must be physically rotated to change directions, which prevents the vehicle from achieving the instantaneous multi-directional movement characteristic of omni-directional robots. This requirement complicates the control systems, increasing the demands on the vehicle's computational and power management systems, and poses challenges for rapid directional changes in dynamic environments.

In response to the limitations presented by traditional and 4WIS4WID mobility systems, as noted in Toyota and Nissan's models, studies from [12] shed light on the advanced mechanisms utilised in omni-directional robots to enhance manoeuvrability beyond these constraints. Omni-directional robots employ specialised wheel designs such as omni-wheels and Mecanum wheels, which allow for movement in any direction without the need for the wheels to physically rotate towards the direction of travel. These wheels feature an array of rollers positioned around their circumference, oriented perpendicularly or at an angle to the main wheel rotation. This unique arrangement enables the wheels to slide laterally with minimal friction while supporting traditional forward and backward movement, thus enabling the robot to execute precise movements in tightly constrained spaces. This mechanical solution directly addresses the core limitation of needing to orient wheels physically before movement can occur, which is a significant challenge in 4WIS4WID systems where each wheel's direction must be adjusted independently. By integrating such omni-directional mechanisms, the foundational mobility of robots is significantly enhanced, allowing for smoother transitions and more efficient navigation in complex environments.

In addition to the mechanisms explored in previous papers like [13], they introduce a refined mechanical approach to enhance vehicle manoeuvrability through the application of Ackerman steering geometry experimentally on a model called Factory Robot (FABOT) vehicle which utilises both four-wheel steer and four independent electric drive systems, enabling highly flexible and dynamic vehicle control. This system employs a unique alignment of steering angles, ensuring that all wheels correctly follow their natural paths during turns. This geometric arrangement minimises the angle discrepancies between the wheels, reducing tyre slippage and wear, which optimises the cornering performance of the vehicle. Previously, Toyota and Nissan models with 4WIS4WID systems were noted for their inability to achieve instant multi-directional movement, largely due to the physical constraints requiring the reorientation of wheels. This can lead to inefficiencies and wear during turns because the wheels may not follow the ideal paths relative to each other. Hence, the Ackerman geometry addresses these issues by ensuring that all wheels are aligned so that they roll correctly through turns, each following its own optimal path. This minimises the tyre slippage and scrubbing that would otherwise occur if the wheels were not properly aligned.

Following the advancements discussed in [13] , where the FABOT vehicle showcased the mechanical capability of four-wheel steering and four independent electric drive systems, studies such as [14] further develop these mechanical foundations. This research elaborates on the application of a 4WID/4WIS system in electric vehicles, enhancing the structural and mechanical design to support complex vehicle dynamics. This development allows each wheel to be not only steered but also driven independently, improving the mechanical flexibility of the vehicle. This means that each wheel is equipped with an in-wheel motor that can operate independently of the others. This means that power can be delivered to each wheel individually based on specific driving needs, such as traction requirements or manoeuvring strategies. This arrangement facilitates more precise handling and superior manoeuvrability, which is crucial for optimising the vehicle's performance in varied driving conditions. By extending the mechanical capabilities of individual wheel control, [14] contributes to the evolution of vehicle design, focusing on maximising the effectiveness and responsiveness of each wheel's contribution to overall vehicle dynamics.

Next, following the advancements highlighted in [14], the study, such as [15] presents a further refined mechanical approach in the realm of compact urban electric vehicles. This research introduces an innovative design that integrates a Four Wheel Independent Steering (4WIS) system with in-wheel drive technology. Each wheel is equipped with its own motor, allowing for independent control of steering and propulsion. This design facilitates a variety of steering modes, including All Wheel Steering (AWS) and Zero Point Turning (ZPT), which drastically improves the vehicle's manoeuvrability in tight urban spaces. The ability to adjust each wheel's angle and torque independently allows the vehicle to execute sharp turns and even rotate in place, overcoming some of the traditional limitations faced by previous vehicle designs in handling and spatial efficiency.

Building upon the mechanical innovations presented in [15], studies such as [16] have presented advances in these concepts further by specifically tailoring the 4WIS system for autonomous ground vehicles. This paper enhances the previous design by integrating sophisticated steer-by-wire modules that not only allow for individual wheel steering but also integrate critical functionalities such as real-time dynamic control of both steering and braking operations. This integration is pivotal for autonomous vehicles, providing them with the ability to perform precise path tracking and advanced manoeuvres through adaptive steering control. Additionally, the mechanical structure is designed to optimise the vehicle's performance in urban environments, focusing on manoeuvrability and stability, which are critical for navigating tight city spaces and complex traffic scenarios.

Expanding on the fundamental understanding of vehicle control mechanisms, it is crucial to explore other aspects in detail, such as steering angle, speed, and autonomous driving [11]. The exploration of 4WIS capabilities and their integration into autonomous driving systems has been significantly advanced through several university-led prototypes, each demonstrating unique mechanical configurations and functionalities. Jilin University's prototype, which achieves a steering angle of ±90° and is capable of speeds up to 8 km/h, has been developed with an emphasis on autonomous

navigation, making it well-suited for urban mobility research. Similarly, the CUHK OK-1 from the Chinese University of Hong Kong, also achieving a ±90° steering angle but slightly faster at 10 km/h, supports autonomous driving, highlighting its potential in testing advanced vehicular dynamics in constrained environments. On the other hand, MIT's Hiriko, with a variable steering range from -60° to +30° and a higher speed capacity of 50 km/h, focuses on manual control mechanisms, offering a unique approach to urban transport solutions without autonomous features. UTM and Tongji University present prototypes designed for practical applications in urban settings, both featuring autonomous driving capabilities with more conservative steering angles of ±35° and ±30°, respectively and speeds of 30 km/h, reflecting their roles in developing efficient transport solutions tailored to real-world conditions. Thus, each researcher's prototype has its own characteristic that is suitable for specific cases.

In order to take more factors into consideration when developing ISBW, the use of exploration in suspension systems is also crucial. According to [11], the diverse suspension types integrated into 4WID-4WIS electric vehicle prototypes are such that each contributes differently to the vehicle's dynamics, with the double wishbone type used in the ROBoMobil exemplifying the optimum choice for handling and stability. This system excels in managing both vertical and lateral forces during high-speed manoeuvres and complex driving scenarios due to its ability to maintain consistent wheel alignment and optimal tyre contact with the road. In contrast, the candle-type suspension, employed by Protean and Tongji, while compact and space-efficient, generally lacks the same level of precision in controlling wheel motion, which can compromise handling and ride quality under dynamic conditions. Similarly, the trailing arm type suspension seen in the Schaeffler prototype provides effective shock absorption and is simpler in construction, but it does not handle lateral stresses as adeptly, which can result in reduced stability during aggressive cornering or when navigating uneven terrain. Each suspension design thus presents a trade-off between simplicity, cost, and performance, with the double wishbone setup offering the best dynamic handling capabilities at the expense of greater complexity and cost.

Moving towards the controllers used in this research, according to [11], it is apparent that the majority of past research on control systems for X-by-Wire mechanisms has primarily relied on simulation testing, with only a select few advancing to the road and Hardware-in-the-Loop (HIL) testing stages. Although these advanced tests have been conducted, the control models employed often utilise only a 2 DOF configuration, which, while common and less complex, may not adequately capture the dynamic intricacies required for more robust real-world applications. This limitation in controller complexity is likely due to the prevalence of this model in academic and initial developmental research, where the focus is often on achieving a proof of concept rather than full operational robustness. Furthermore, most past researchers have confined their validation to simulation environments, typically employing 2 to 3 DOF in their control strategies. This approach suggests a cautious progression in research development, where the complexity of controllers presents significant challenges in transitioning from theoretical models to practical testing environments such as HIL or road tests. There is a clear need for more comprehensive development and testing that moves beyond common, simpler control models to embrace more complex systems capable of handling the nuances of real-world driving dynamics.

Taking into consideration the research findings, this project presents significant potential to advance ISBW technology to tackle all the issues from the previous paper, either from a design perspective or the control system itself. This paper delineates the enhancement in DOF employed in vehicle dynamics studies from the conventional 2DOF and 3DOF to a more intricate 14-DOF approach. Previous research typically incorporated common control models; however, this study recognises the complexity and the advanced technological demands of modern vehicles, necessitating a comprehensive and detailed dynamic analysis. Notably, while the existing literature predominantly presents simulations of advanced control systems, this work extends beyond simulation, incorporating road tests to validate the controllers. This research significantly advances the domain of automotive steering systems, laying a robust foundation for future innovations and promising safer, more efficient, and responsive steering mechanisms, thereby contributing to the transformative progression of the automotive experience. Through the development of advanced control algorithms, a notable achievement is realised: enabling the SBW system to independently regulate the steering angle of each wheel. This advancement marks a pivotal shift, promising enhanced vehicle manoeuvrability and agility, with potential benefits including reduced turning radius and improved lane-change capabilities. Moreover, this project introduces a groundbreaking theoretical framework based on Model Reference Adaptive Control (MRAC). Leveraging MRAC algorithms for predictive control, this approach represents a significant step forward in proactive steering adjustments. By anticipating road conditions and driver intentions, the SBW system can proactively adjust steering angles based on sensor inputs and real-time environmental cues. This predictive capability holds tremendous promise for refining vehicle stability and responsiveness, paving the way for a safer and more adaptable driving experience.

This paper is divided into five sections that cover different but interconnected aspects of SBW technology in electric vehicles. The first section provides a brief background to the study, including a review of previous work on SBW systems and an evaluation of current SBW performance metrics. In the second section, the focus shifts to the technical core of the study, introducing the mathematical equations needed for developing the simulation model, along with detailed explanations of the hardware, instrumentation, and data acquisition systems used in the experimental study. This section also includes information on determining the vehicle's centre of gravity. The third section discusses the control strategy and the simulation parameters assigned to the SBW system. The fourth section presents the results obtained from both the simulation study and the experimental study, displaying the practical outcomes of the research. Finally, the paper concludes in the fifth section, synthesising the study's findings, drawing conclusions that encapsulate the key findings and identifying the implications for future advancements in SBW technology.

2. MATHEMATICAL DESCRIPTION OF VEHICLE EMPLOYING INDEPENDENT STEER BY WIRE

In general, the proposed independent steering system (ISS) mechanism was a cutting-edge development that integrates two separate systems, namely the steering wheel and integrated suspension-steering arm subsystems. Mechanically, the steering wheel subsystem motor consists of the steering wheel, steering column, bearing, and direct current (DC) motor, which is responsible for controlling the direction of the vehicle. On the other hand, for the road wheel steering arm subsystems, the mechanism consists of an integrated suspension and steering system arm that responsible for steering the wheel, which can be categorised as the core mechanism in this SBW development. It comprised of a DC motor, gears, shaft, integrated suspension-steering arms, and wheel. By maintaining the same objective, these two SBW subsystems have been utilised by replacing the conventional steering systems that used in the Carsim Software vehicle which is then used as the benchmark as shown in Figure 1.

Due to the capability of the ISS to improve the vehicle's dynamic performance, a mathematical simulation was conducted using MATLAB/Simulink with a 14-DOF full-vehicle model. The model consists of a 7DOF ride model, namely the roll, pitch and vertical motion of each of the four wheels, as well as seven degrees of freedom handling model, namely longitudinal, lateral, vertical and rotational motion of the wheels. To justify this modelling, some assumptions have been made which are: the vehicle body is lumped into a single mass which is referred to as the sprung mass, aerodynamic drag force is ignored and the roll centre is coincident with the pitch centre and located at just below the body centre of gravity. The suspensions located at the arm are modelled as passive viscous dampers and spring elements that are mounted at the suspension-steering arm. Although the suspension system has a 30-degree tilt angle towards the vertical axis, for the purposes of this analysis, it is assumed that this tilt angle does not significantly affect the dynamics of the vehicle because it is mathematically proven that ($\cos 30^{o} \approx 1$). This assumption is based on the context that the primary dynamics of interest in this analysis are those in which the influence of the tilt angle is considered negligible, such as low-speed manoeuvres or within the specific range of typical operating conditions where previous studies have shown minimal impact. Aside from that, it was also assumed that the rolling resistance effect was neglected as the passive stabiliser bar was not in use and body flexibility was neglected. The vehicle remains grounded at all times and the four tyres never lose contact with the ground during manoeuvring. Tyre vertical behaviour is represented as a linear spring without damping, whereas the lateral and longitudinal behaviours are represented with a magic formula tyre model.

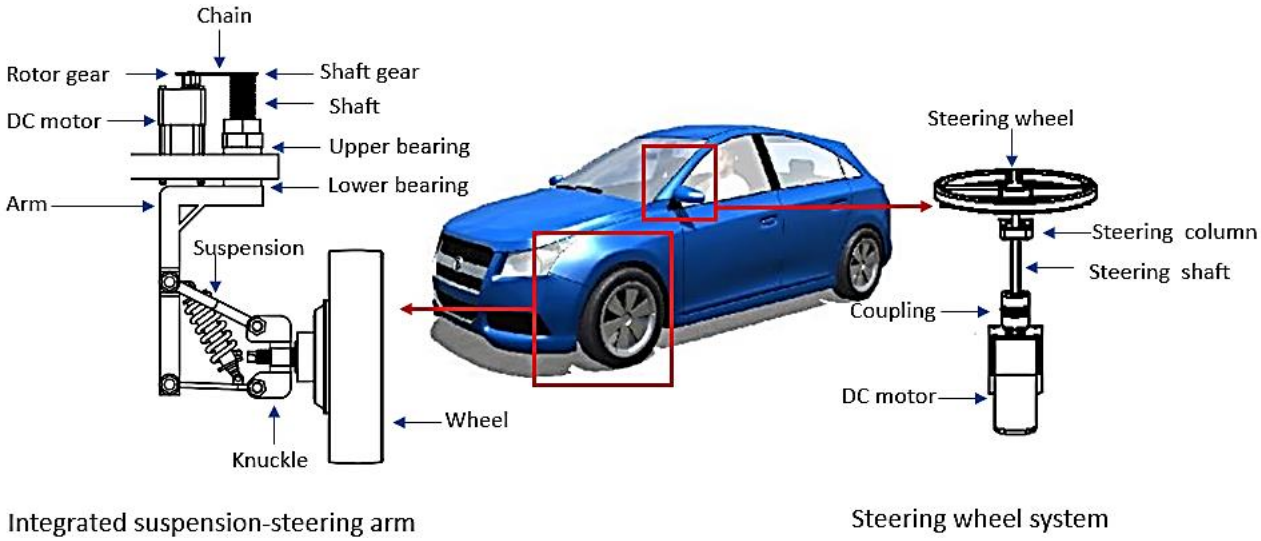

Figure 1. The ISBW implemented in a vehicle

2.1 Seven Degrees of Freedom for Ride Model

Figure 2 shows a free-body diagram of a 7-DOF system. It consists of a single sprung mass (car body) connected to four unsprung masses (front-left, front-right, rear-left and rear-right wheels) at each corner. The sprung mass is free to heave, pitch and roll, while the unsprung masses are free to bounce vertically with respect to the sprung mass. The suspensions between the sprung mass and unsprung masses are modelled as passive viscous dampers and spring elements. The tyres are modelled as simple linear springs without damping. For simplicity, all pitch and roll angles are assumed to be small. A similar model was used in [17].

Referring to Figure 2, the force balance, rolling and pitching acting on sprung mass mathematically can be described in equations (1), (2) and (3) respectively:

$$M_s \ddot{Z}_s = F_{sfl} + F_{dfl} + F_{sfr} + F_{dfr} + F_{srl} + F_{drl} + F_{srr} + F_{drr} \quad (1)$$

where:

M_s = sprung mass weight

$\ddot{Z}_s$ = sprung mass acceleration at body centre of gravity (CG)

$F_{sfl} = K_{sfl}(Z_{ufl} - Z_{sfl})$ = front left spring force

$F_{sfr} = K_{sfr}(Z_{ufr} - Z_{sfr})$ = front right spring force

$F_{srl} = K_{srl}(Z_{url} - Z_{srl})$ = rear left spring force

$F_{srr} = K_{srr}(Z_{urr} - Z_{srr})$ = rear right spring force

$F_{dfl} = C_{sfl}(\dot{z}_{ufl} - \dot{Z}_{sfl})$ = front left damper force

$F_{dfr} = C_{sfr}(\dot{z}_{ufr} - \dot{Z}_{sfr})$ = front right damper force

$F_{drl} = C_{srl}(\dot{z}_{url} - \dot{Z}_{srl})$ = rear left damper force

$F_{drr} = C_{srr}(\dot{z}_{urr} - \dot{Z}_{srr})$ = rear right damper force

whilst

K_{sfl}, K_{sfr}, K_{srl} and K_{srr} = spring stiffness at the front left, front right, rear left and rear right respectively

C_{sfl}, C_{sfr}, C_{srl} and C_{srr} = damping stiffness at the front left, front right, rear left and rear right respectively

Z_{sfl}, Z_{sfr}, Z_{srl} and Z_{srr} = sprung masses verticle displacement at the front left, front right, rear left and rear right respectively

$\dot{Z}_{sfl}$, $\dot{Z}_{sfr}$, $\dot{Z}_{srl}$ and $\dot{Z}_{srr}$ = sprung masses verticle velocity at the front left, front right, rear left and rear right respectively

Z_{ufl}, Z_{ufr}, Z_{url} and Z_{urr} = unsprung masses verticle displacement at the front left, front right, rear left and rear right respectively

$\dot{z}_{ufl}$, $\dot{z}_{ufr}$, $\dot{z}_{url}$ and $\dot{z}_{urr}$ = unsprung masses verticle velocity at front left, front right, rear left and rear right respectively

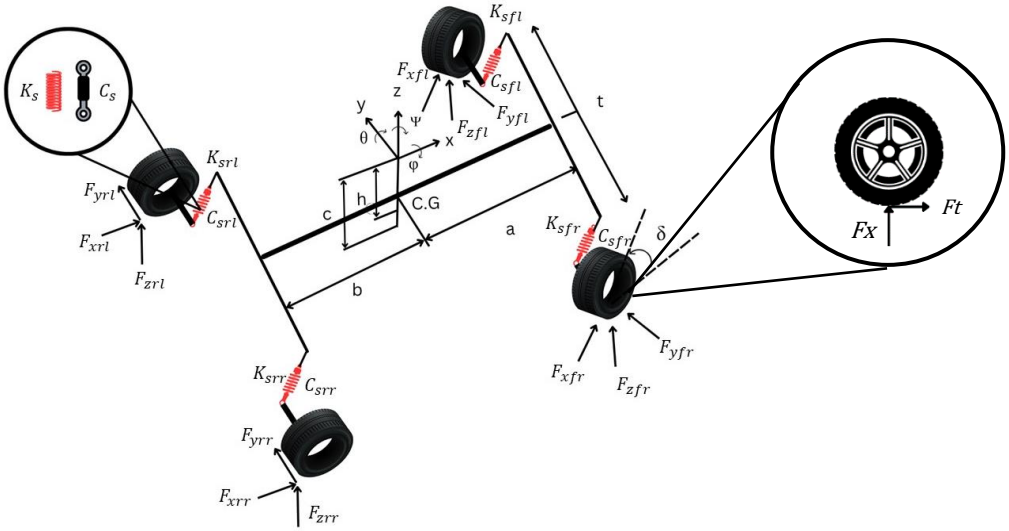

Figure 2. A 14-DOF full-vehicle ride and handling model

Similarly, the moment balance equation for roll motion acting on the x-axis and pitch motion acting on the y-axis are given as equations (2) and (3) correspondingly such as follows:

$$I_\varphi \ddot{\varphi} = [F_{sfl} + F_{dfl} + F_{srl} + F_{drl}]\frac{t}{2} - [F_{sfr} + F_{dfr} + + F_{srr} + F_{drr}]\frac{t}{2} \quad (2)$$

$$I_\theta \ddot{\theta} = [F_{sfl} + F_{dfl} + F_{sfr} + F_{dfr}]a - [F_{drr} + F_{drl} + F_{srr} + F_{drr}]b \quad (3)$$

where:

$\ddot{\varphi}$ = the roll acceleration at CG

$\ddot{\theta}$ = the pitch acceleration at CG

I_φ = the roll moment of inertia

I_θ = the pitch moment of inertia

t = the track width

a = the distance between the front axle to CG

b = the distance between rear axle to CG

Note that the sprung mass position at each corner can be expressed in terms of bounce, pitch and roll, which then can be expressed as:

$$\begin{aligned} Z_{sfl} &= Z_s + \frac{t}{2}\varphi - a\theta\ ; \quad \dot{Z}_{sfl} = \dot{Z}_s + \frac{t}{2}\dot{\varphi} - a\dot{\theta} \\ Z_{sfr} &= Z_s - \frac{t}{2}\varphi - a\theta\ ; \quad \dot{Z}_{sfr} = \dot{Z}_s - \frac{t}{2}\dot{\varphi} - a\dot{\theta} \\ Z_{srl} &= Z_s + \frac{t}{2}\varphi + b\theta\ ; \quad \dot{Z}_{srl} = \dot{Z}_s + \frac{t}{2}\dot{\varphi} + b\dot{\theta} \\ Z_{srr} &= Z_s - \frac{t}{2}\varphi + b\theta\ ; \quad \dot{Z}_{srr} = \dot{Z}_s - \frac{t}{2}\dot{\varphi} + b\dot{\theta} \end{aligned} \tag{4}$$

Here, φ is the body roll angle, whereas θ is the body pitch angle at the body centre of gravity.

Apart from the three motions that act on the sprung mass, there are another four motions that exist and act on the unsprung mass, which then can be categorised as the ability of unsprung mass to be dynamic in the vertical direction in every corner of the vehicle. Mathematically, it can be described as equations (5) to (8).

$$M_{ufl}\ddot{Z}_{ufl} = F_{tfl} - F_{sfl} - F_{dfl} \tag{5}$$

$$M_{ufr}\ddot{Z}_{ufr} = F_{tfr} - F_{sfr} - F_{dfr} \tag{6}$$

$$M_{url}\ddot{Z}_{url} = F_{trl} - F_{srl} - F_{drl} \tag{7}$$

$$M_{urr}\ddot{Z}_{urr} = F_{trr} - F_{srr} - F_{drr} \tag{8}$$

where, the normal force (F_z) is assumed to be the same as tyre force (F_t) and can be described as:

$F_{tfl} = K_{tfl}(Z_{rfl} - Z_{ufl})$ = front left tyre force
$F_{tfr} = K_{tfr}(Z_{rfr} - Z_{ufr})$ = front right tyre force
$F_{trl} = K_{trl}(Z_{rrl} - Z_{url})$ = rear left tyre force
$F_{trr} = K_{trr}(Z_{rrr} - Z_{urr})$ = rear right tyre force

while,

M_{ufl}, M_{ufr}, M_{url} and M_{urr} = unsprung mass at the front left, front right, rear left and rear right respectively
K_{tfl}, K_{tfr}, K_{trl} and K_{trr} = tyre stiffness at the front left, front right, rear left and rear right respectively
Z_{rfl}, Z_{rfr}, Z_{rrl} and Z_{rrr} = road profile applied to the front left, front right, rear left and rear right tyres respectively

2.2 Seven Degrees of Freedom for Handling Model

To complete the other 7-DOF, the handling model will be looked at in Figure 3. The model considers three degrees of freedom (DOF) due to lateral and longitudinal movements, as well as a yaw motion related to the vehicle body (r) and an additional DOF for each tyre's rotational motion. It assumes the vehicle operates on a flat road. The vehicle experiences motion along the x-axis (longitudinal) and y-axis (lateral), as well as angular yaw motions around the vertical z-axis. In the horizontal plane, the vehicle's motion is characterised by longitudinal (a_x) and lateral (a_y) accelerations, and by velocities in the longitudinal (v_x) and lateral (v_y) directions. The total vehicle mass is represented by m_t, while the steering angle and yaw rate are denoted by δ and $\dot{r}$ respectively.

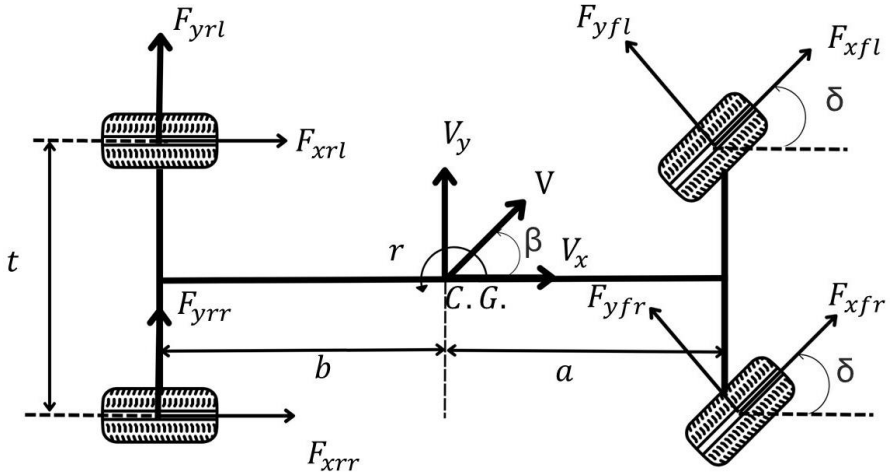

Figure 3. A 7-DOF vehicle handling model

The derivation of acceleration in the longitudinal x-axis is as follows:

$$\dot{x} = \ddot{x} + \dot{y}\dot{\psi} \tag{9}$$

One way to calculate longitudinal acceleration is by adding up all the forces acting in the x-axis direction as follows:

$$M_t\ddot{x} = F_{xfl}\cos\delta + F_{yfl}\sin\delta + F_{xfr}\cos\delta + F_{yfr}\sin\delta + F_{xrl} + F_{xrr} \tag{10}$$

Acceleration in the lateral y-axis will appear similar to acceleration in the longitudinal x-axis.

$$\dot{y} = \ddot{y} + \dot{x}\dot{r} \tag{11}$$

One way to calculate lateral acceleration is by adding up all the forces acting in the y-axis direction as follows:

$$M_t\ddot{y} = F_{yfl}\cos\delta - F_{xfl}\sin\delta - F_{yfr}\cos\delta - F_{xfr}\sin\delta + F_{yrl} + F_{yrr} \tag{12}$$

The equation of motion for yaw is expressed by the following formula, in which the aligning moment Mz is assumed to have the same direction as the yaw motion.

$$\begin{aligned} I_\psi\ddot{\Psi} = &\left(-F_{xfl}\cos\delta + F_{xfr}\cos\delta - \ddot{F_{xrl}} + F_{xrr} + F_{yfl}\sin\delta - F_{yfr}sin\delta\right)\frac{t}{2} \\ &+\left(F_{xfl}sin\delta + F_{yfl}cos\delta + F_{xfr}sin\delta + F_{yfr}cos\delta\right)a - \left(F_{yrl} + bF_{yrr}\right)b \\ &+M_{zfl} + M_{zfr} + M_{zrl} + M_{zrr} \end{aligned} \tag{13}$$

where:

$\ddot{x}$	=the longitudinal acceleration at CG
$\ddot{y}$	=the lateral acceleration at CG
$\ddot{\psi}$	= yaw acceleration
ψ	= yaw angle
$\dot{x}$	= the longitudinal velocity at CG
$\dot{y}$	= the lateral velocity at CG
I_ψ	= the yaw moment of inertia
M_t	= total mass of the vehicle
δ	= wheel steer angle
F_{xfl}, F_{xfr}, F_{xrl} and F_{xrr}	= unsprung mass at the front left, front right, rear left and rear right respectively
F_{yfl}, F_{yfr}, F_{yrl} and F_{yrr}	= tyre stiffness at the front left, front right, rear left and rear right respectively
M_{zfl}, M_{zfr}, M_{zrl} and M_{zrr}	= road profile applied to the front left, front right, rear left and rear right tyres respectively

Note that the $\dot{x}$ and $\dot{y}$ are used to obtain the tyre side slip angle, denoted by α which can be found as:

$$\alpha_f = \tan^{-1}\left(\frac{\dot{y} + ar}{\dot{x}}\right) - \delta_f \tag{14}$$

and

$$\alpha_r = \tan^{-1}\left(\frac{\dot{y} - br}{\dot{x}}\right) \tag{15}$$

wherein α_f and α_r are the side slip angles at the front and rear tyres, respectively. The front and rear longitudinal velocity components are given by:

$$v_{wxij} = V_{tij}\cos\alpha_{ij} \tag{16}$$

where, the speed of the wheels is,

$$V_{tij} = \sqrt{\left(v_y + l_f r\right)^2 + v_x^2} \tag{17}$$

then, the longitudinal slip ratio of the tyres,

$$s_{af} = \frac{v_{wxij} - \omega_{ij}R_w}{v_{wxij}} \tag{18}$$

where ω_{ij} represents the angular velocity of any tyre, and R_w is the wheel radius. Meanwhile, '*i*' and '*j*' indicate front, rear, and left or right tyre, respectively.

The degree of freedom of the tyre spin is measured by the wheel angular velocity, ω, as shown in Figure 4. The equation represents the assumption that the car is front-wheel drive where T_d is driving torque, T_b is braking torque, T_{rr}

is rolling resistance torque, T_{tr} is traction torque and R_w is radius wheel. The total torque around the wheel axle for each wheel can be calculated using the following equation.

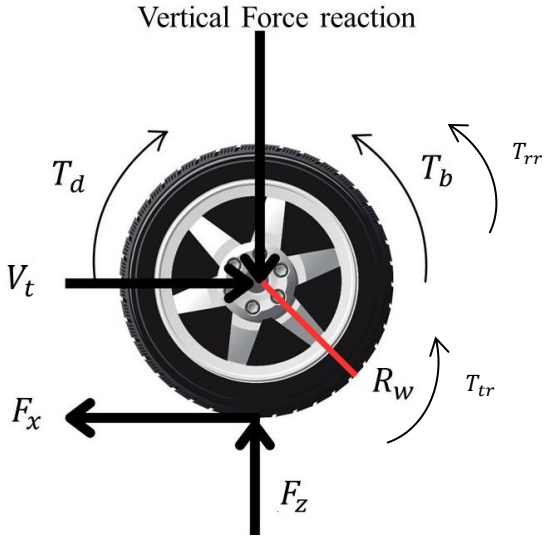

Figure 4. FBD of a wheel

$$I_\omega \ddot{\omega}_{fl} = T_{dfl} - T_{bfl} - T_{rrfl} - T_{trfl} \quad (19)$$

$$I_\omega \ddot{\omega}_{fr} = T_{dfr} - T_{bfr} - T_{rrfr} - T_{trfr} \quad (20)$$

$$I_\omega \ddot{\omega}_{rl} = -T_{brl} - T_{rrrl} - T_{trrl} \quad (21)$$

$$I_\omega \ddot{\omega}_{rr} = -T_{brr} - T_{rrrr} - T_{trrr} \quad (22)$$

where

$$T_{tr} = F_x(R_w) \quad (23)$$

$$F_x = \mu(F_z) \quad (24)$$

$$F_z = -mg \quad (25)$$

2.2.1 Tyre model

Tyres are considered to be one of the most crucial and complex components of a vehicle, as stated in [22]. In addition to providing support to the vehicle and minimising the impact of road irregularities, tyres also play a vital role in generating longitudinal and lateral forces needed to alter the vehicle's speed and direction. These forces are generated by the tyre's deformation when it comes in contact with the road during cornering, acceleration, and braking. Figure 5 shows the fundamentals of tyre dynamics. In the tyre model, F_y and F_x represent the forces that impact the tyre laterally and longitudinally, respectively. These forces are crucial in understanding the tyre's grip during cornering, acceleration, and braking. The aligning moment, M_z, is an important parameter that reflects the self-aligning torque and contributes to steering response and stability. The slip angle α represents the angle between the tyre's direction and its actual path of travel, which is a critical factor in vehicle handling dynamics. Finally, the symbol '*v*' signifies the tyre's forward velocity, and it is necessary to determine the effects of other variables on tyre performance. The Pacejka model uses these parameters to predict tyre behaviour, which is fundamental for simulations of vehicle dynamics. The simplified equations using the Pajecka model are shown.

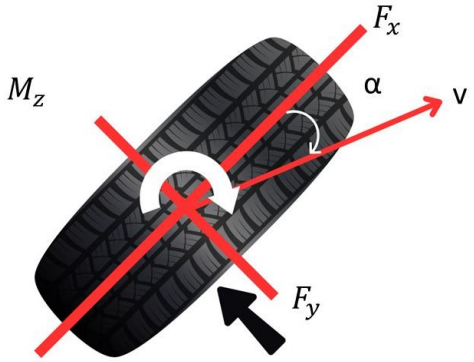

Figure 5. Tyre dynamic while at a slip angle

Table 1. Coefficients for tyre formula with load influence

	a_1	a_2	a_3	a_4	a_5	a_6	a_7	a_8
F_y	-22.1	1011	1078	1.82	0.208	0.000	-0.354	0.707
M_z	-2.72	-2.28	-1.86	-2.73	0.110	-0.070	0.643	-4.04
F_x	-21.3	1144	49.6	226	0.069	-0.006	0.056	0.486

Table 2. Coefficient for tyre formula with camber influence

	a_9	a_{10}	a_{11}	a_{12}	a_{13}
F_y	0.028	0.000	14.8	0.022	0.000
M_z	0.015	-0.066	0.945	0.030	0.070

Equations (26) to (35) are used to determine the lateral force F_y. The calculations are slightly influenced by the camber angle, γ, which is measured in degrees. The shape factors and the slip angle, α, are the key variables that determine the amount of lateral force. Keep in mind that when applied to the ISO standard vehicle model, the sign of the lateral force must be reversed to conform to the ISO standard definition of slip angle.

$$C = 1.30 \tag{26}$$

$$D = a_1 {F_z}^2 + a_2 F_z \tag{27}$$

$$BCD = a_3 \sin\left(a_4 tan^{-1}(a_5 F_z)\right) \tag{28}$$

$$B = \frac{BCD}{CD} \tag{29}$$

$$E = a_6 {F_z}^2 + a_7 F_z + a_8 \tag{30}$$

$$S_h = a_9 \gamma \tag{31}$$

$$S_v = (a_{10} {F_z}^2 + a_{11} F_z)\gamma \tag{32}$$

$$\Delta B = -a_{12} |\gamma| B \tag{33}$$

$$\emptyset = (1 - E)(\alpha + S_h) + \frac{E}{B} tan^{-1}(B(\alpha + S_h)) \tag{34}$$

$$F_y = D sin\left(C tan^{-1}(B\emptyset)\right) + S_v \tag{35}$$

In order to find the aligning moment M_z, the equations can be written as (36) to (46).

$$C = 2.40 \tag{36}$$

$$D = a_1 {F_z}^2 + a_2 F_z \tag{37}$$

$$BCD = \frac{a_1 {F_z}^2 + a_4 F_z}{e^{a_5 F_z}} \tag{38}$$

$$B = \frac{BCD}{CD} \tag{39}$$

$$E = a_6 {F_z}^2 + a_7 F_z + a_8 \tag{40}$$

$$S_h = a_9 \gamma \tag{41}$$

$$S_v = (a_{10} {F_z}^2 + a_{11} F_z)\gamma \tag{42}$$

$$\Delta B = -a_{12} |\gamma| B \tag{43}$$

$$\Delta E = \frac{E}{1 - a_{13}|\gamma|} - E \tag{44}$$

$$\emptyset = (1 - E)(\alpha + S_h) + \frac{E}{B} tan^{-1}(B(\alpha + S_h)) \tag{45}$$

$$M_z = Dsin\big(Ctan^{-1}(B\emptyset)\big) + S_v \tag{46}$$

Equations (47) to (53) are used to determine the longitudinal force F_x. Keep in mind that the longitudinal force depends on the shape factors and the percentage of longitudinal slip, σ.

$$C = 1.65 \tag{47}$$

$$D = a_1 {F_z}^2 + a_2 F_z \tag{48}$$

$$BCD = \frac{a_3 {F_z}^2 + a_4 F_z}{e^{a_5 F_z}} \tag{49}$$

$$B = \frac{BCD}{CD} \tag{50}$$

$$E = a_6 {F_z}^2 + a_7 F_z + a_8 \tag{51}$$

$$\emptyset = (1 - E)\sigma + \frac{E}{B} tan^{-1}(B\sigma) \tag{52}$$

$$F_x = Dsin(Ctan^{-1}(B\emptyset)) \tag{53}$$

Equation (54) shows that α represents the slip angle, v_y represents the lateral velocity, v_x represents the longitudinal velocity, and δ represents the steering angle. It is important to note that equation (54) uses a small angle approximation, where the steering angle δ is assumed to be the same as the angle of the velocity vector of the front axle relative to the vehicle. To calculate the slip angle α, the lateral velocity v_y and the longitudinal velocity v_x are used as follows:

$$\alpha = \arctan(\frac{v_y}{v_x}) - \delta \tag{54}$$

The longitudinal slip is related to the rotation of the wheels relative to the vehicle's longitudinal (forward) motion and is denoted by σ. The longitudinal slip ratio is used to determine the amount of traction between the tyre and the road surface. It is defined differently depending on whether the wheel is braking or driving. In practice, the slip ratio σ should not exceed 1 (or 100%) because a slip ratio greater than one would imply that the tyre is skidding without any longitudinal force being transmitted between the tyre and the road. To prevent the slip ratio from exceeding certain bounds, a min/max function is sometimes applied to keep it within the physical limits where v_{xw} is the free-rolling longitudinal velocity of the wheel and v_x is the actual longitudinal velocity of the vehicle. Thus, the slip equation can be defined by:

$$\sigma = \frac{v_{xw} - v_x}{\max, \min\,(v_{xw}, v_x)} \tag{55}$$

2.3 Modelling Proposed ISBW System

The steering system will comprise two distinct parts. The first part of the system will be responsible for controlling the direction of the vehicle and will include a steering wheel, steering column, bearing, and motor. The second part of the system will consist of an arm responsible for steering the tyre. This arm will be comprised of a motor, gears, chains, shaft, swing arms, suspension, and tyre. The SBW system is mathematically modelled using Newton's Second Law, a fundamental law of physics that describes how forces interact with objects. According to this law, the force applied to an object produces acceleration proportional to the object's mass. In the case of rotational motion, the moment of inertia (a measure of an object's resistance to rotational acceleration) is also taken into account. Next, the arm that steers the wheel also uses the same principle as the steering wheel model, but in this case, an assumption has been made that the shaft and arm are connected; in other words, it is one rigid body. The ratio between the gear from the motor to the shaft's gear is considered 1:1. Hence, once the motor is rotating, the shaft that connects the arm also rotates. Figure 6 shows FBD for the proposed prototype model. This model helps to accurately predict the behaviour of the SBW system and ensures that it operates safely and efficiently.

2.3.1 Steering wheel dynamics

The steering wheel dynamics system comprises three main components: the steering wheel, steering column, and DC motor. The mathematical equation for this system is based on Newton's second law. The dynamic model of a steering system incorporates the effects of inertia, stiffness, damping, and external torques. Below are the steps to derive such an equation:

$$J_{sw}\ddot{\theta}_{sw} = T_{sw} - K_{sc}(\theta_{sw} - \theta_{ms}) - B_{sc}\big(\dot{\theta}_{sw} - \dot{\theta}_{ms}\big) - T_{ms} - B_{ms}(\dot{\theta}_{ms}) \tag{56}$$

where:

J_{sw} = The moment of inertia of the steering wheel
$\ddot{\theta}_{sw}$ = Angular acceleration of the steering wheel
T_{sw} = The torque applied to the steering wheel
K_{sc} = The spring stiffness of the steering column
θ_{sw} = Angle of the steering wheel
θ_{ms} = Angle of the motor steering wheel
B_{sc} = The damping coefficient of the steering column
$\dot{\theta}_{ms}$ = The angular velocity of the motor steering
T_{ms} = The torque on the motor steering
B_{ms} = The damping coefficient of motor steering

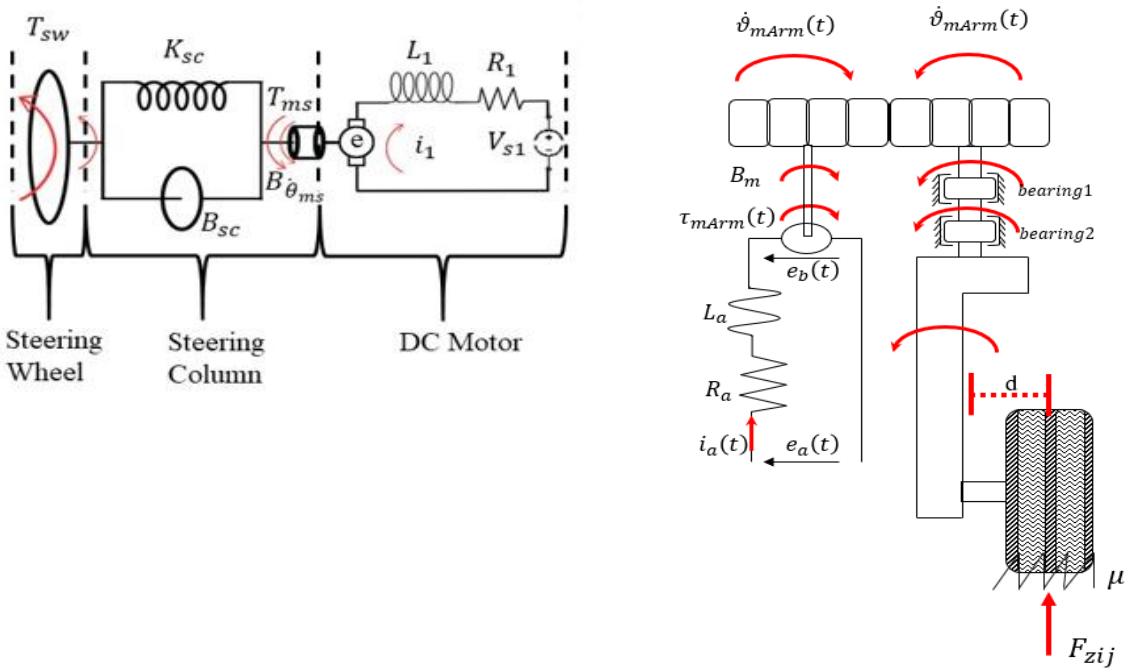

Figure 6. FBD for the proposed system

Equation (56) shows how to find the sum of moments (torques) acting on the steering. The total torque acting on the steering wheel comes from three sources: the driver, the DC motor, and any resistance (like friction). The moment of inertia J_{sw} describes the steering wheel's resistance to changes in its rotational speed, calculated by multiplying it with the angular acceleration $\ddot{\theta}_{sw}$ to determine the required torque to alter the steering speed. The damping coefficient B_{sc} represents the resistance to motion from the steering column's own materials and connections to the rest of the steering system. It is multiplied by the angular velocity $\dot{\theta}_{sw}$ to get the damping torque. The steering system has feedback in the form of resistance to turning, modelled here with a spring (with spring constant K_{sc}) that measures the difference between the steering wheel angle θ_{sw} and the θ_{ms}. This creates a restoring torque that tries to bring the steering wheel back to its original position when the driver is not exerting any force. Friction from the DC motor also opposes the motion of the steering wheel, represented by T_{ms}, and its direction is indicated by the angular velocity of the DC motor $\dot{\theta}_{ms}$. Putting all these together, the equation balances the torque generated by the driver T_{sw} with the inertial, elastic, and damping effects of the steering system, along with any additional torques acting on the mechanism T_{ms}. This dynamic model helps in understanding how the steering wheel's motion is transferred to the tyres and how various forces interact to influence the steering behaviour of a vehicle.

2.3.2 Integrated suspension steering arm of ISBW system model

The system that controls the independent arm dynamics consists of three main components: a DC motor, shaft, and arm. The mathematical equation that describes this system is based on Newton's second law and considers the effects of inertia, stiffness, damping, and external torques. However, some assumptions have been made to simplify the mechanism. Firstly, the ratio between the steering wheel angle (θ_{sw}) and the angle of the arm (δ_{arm}) is assumed to be 1:21. Secondly, since the tyre is attached to the arm, the angle of the tyre (δ_{tire}) is assumed to be the same as the angle of the arm (δ_{tire}). Equations (57) and (58) are the mathematical expressions describing the DC motor, shaft, and arm components of the system.

$$J_{total}\ddot{\delta} = \tau_{mArm} - B_{mArm}(\dot{\vartheta}_{mArm}) - K_{tmArm}(\vartheta_{mArm}) - B_{bearing1}(\dot{\delta}) \\ -K_{bearing1}(\delta) - B_{bearing2}(\dot{\delta}) - K_{bearing2}(\delta) + \mu F_{zij}(d) - M_{zij} \quad (57)$$

The electric equation for the motor is based on Kirchhoff's voltage law and is elaborated as:

$$L\frac{di_a}{dt} + R_a i_a = e_a \dot{\vartheta}_{mArm} \quad (58)$$

where

τ_{mArm} = $K_{tarm} i_a$ = motor arm torque
J_{total} = $J_{mArm} + J_{Arm}$
J_{mArm} = moment inertia of the motor arm
J_{Arm} = total integrated suspension-steering arm inertia
K_{tmArm} = motor arm stiffness
$K_{bearing1}$ = arm upper bearing stiffness
$K_{bearing2}$ = arm lower bearing stiffness
B_{mArm} = motor arm damping coefficient
$B_{bearing1}$ = arm upper bearing stiffness
$K_{bearing2}$ = arm lower bearing stiffness
$\dot{\vartheta}_{mArm}$ = motor arm angular velocity
ϑ_{mArm} = motor arm angular displacement
$\ddot{\delta}$ = wheel steer angular acceleration
$\dot{\delta}$ = wheel steer angular velocity
δ = wheel steer angular displacement
F_{zfi} = normal force at the front tyre, where i indicates left or right tyre
d = distance of contact patch of the tyre to the centre of the arm shaft
M_{zfi} = front wheel self-aligning moment, where i indicates the left or the right tyre
R_a = motor electric resistance
i_a = motor arm armature current
L = motor electric inductance
e_a = motor back electromotive force (back emf)

It is important to keep in mind that Equation (57) is a generalised equation, meaning that it may differ for other positions such as the front left, front right, rear left, and rear right tyres [18]-[20]. Each tyre's unique position may require a specific equation to accurately represent its behaviour.

2.4 Full Vehicle Model Integrated with ISBW Subsystem and Parameter

Once the 14 DOF equations for the vehicle dynamics and the specific equation for the proposed steering system have been derived, the next step is to translate them into a computational model. This is achieved using MATLAB/Simulink, a simulation and modelling tool designed to simulate, analyse and design systems that involve dynamic feedback. The Simulink model is a graphical representation of the mathematical equations, which are encapsulated in interconnected blocks that simulate the real-time behaviour of the vehicle's steering response and overall dynamics. These blocks represent the derived equations and system components and are systematically arranged to offer a platform for further analysis, testing, and validation of the theoretical models. To provide a visual guide for the proposed configuration of the Simulink model, Figure 7 illustrates how the blocks are arranged to simulate the dynamic interactions and feedback loops of the system. When building a model for vehicle dynamics in MATLAB/Simulink, it is important to differentiate between constant and variable parameters. The parameters that remain static regardless of the driving conditions, such as mass, wheel track, wheel base, and other static geometric properties, will be inputted directly into the Simulink model as fixed values. These constants serve as the foundation of the simulation, providing a stable framework to develop the vehicle's dynamics.

On the other hand, parameters that can change during driving, such as vertical tyre forces, slip angles, aerodynamic forces, and others will not be statically defined in the model. Instead, these parameters will be introduced into the simulation as time-varying inputs or through lookup tables that encapsulate the range of their operational states. This ensures that the model can accurately replicate the dynamic behaviour of the vehicle under different conditions. All values for the constant parameters will be set according to the default specifications provided by CarSim. The reason behind using CarSim as the source of reference is that this software has been widely used by other researchers, such as in this recent research [21]. This approach ensures that the simulation reflects realistic vehicle responses and interactions as the baseline for analysis. By doing so, the model maintains fidelity to real-world vehicle dynamics, allowing for more reliable predictions and assessments of vehicular behaviour within the simulated environment. The parameters of the vehicle utilised in the simulation are listed in Table 3.

Table 3. Full vehicle model parameters based on CarSim

Parameter	Symbol	Value
Mass vehicle	m	833kg
Track width	t	1.415m
Wheelbase	l	2.35m
Distance front axle to CG	a	1.1m
Distance rear axle to CG	b	1.25m
Suspension damping coefficient front	C_{df}	1.032
Suspension damping coefficient rear	C_{dr}	1.032
Frontal area of the vehicle	A	$1.6m^3$
Suspension spring stiffness front	K_{sf}	$18000N/m$
Suspension spring stiffness front	K_{sr}	$18000N/m$
Distance from ground to CG	h	0.54m
Moment of roll	I_{φ}	$270kg.m^2$
Moment of pitch	I_{θ}	$750kg.m^2$
Mass wheel	M_w	20.75kg
The spring stiffness of the steering column	K_{sc}	$3500N/m$
The damping coefficient of the steering column	B_{sc}	0.0035
Damping due to the motor	B_m	1
Torque constant of the motor	K_m	$3N/m$
Damping coefficient of the bearing 1	B_{b1}	1000
Stiffness of the bearing 1	K_{b1}	$1000N/m$
Damping coefficient of the bearing 2	B_{b2}	1000
Stiffness of the bearing 2	K_{b2}	$1000N/m$
Displacement from the centre tyre to centre of the shaft	d	0.85m

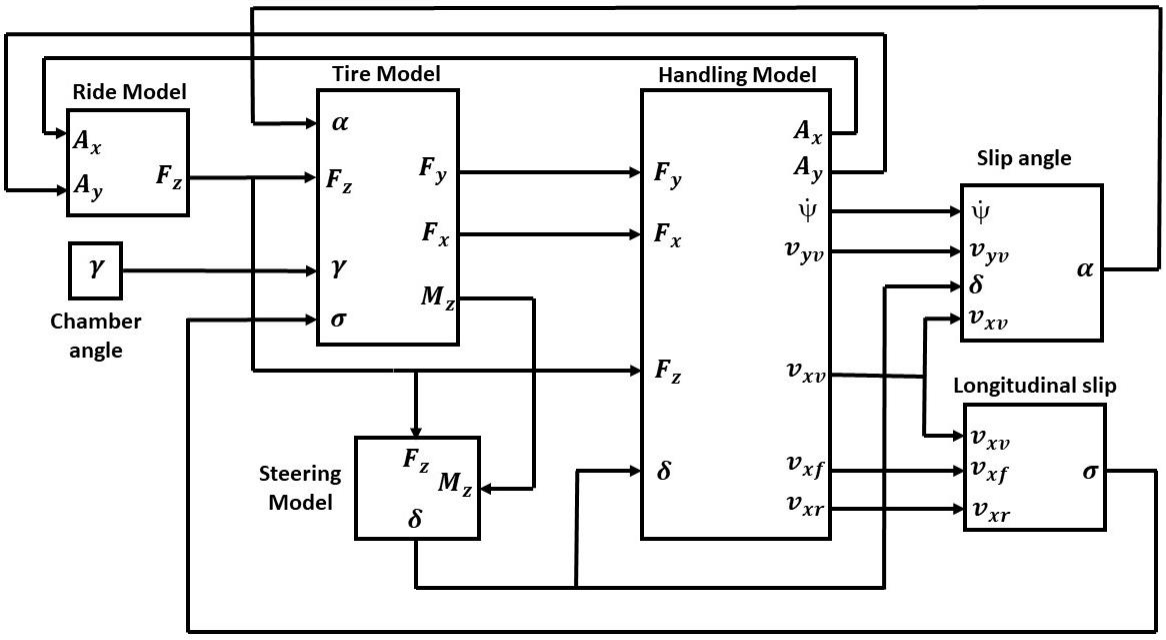

Figure 7. Full vehicle model in MATLAB-SIMULINK

3. MRAC CONTROL STRATEGY

This section focuses on the control strategy for the steering system. It is insightful to observe the evolution of control techniques applied to optimise system performance. Initially, a conventional Proportional-Integral-Derivative (PID) controller was implemented. To effectively manage an error, it is necessary to control its present state, as well as its past and future occurrences. This involves monitoring and adjusting the error in proportion to its current value (proportional), its accumulation over time (integral), and its rate of change (derivative) [23]. Although the PID controller is widely used in industry due to its simplicity and robustness, it has not been able to produce satisfactory results for the complex dynamics of the steering system. Past research has stated that the PID controller needs to be combined with other controllers that have more complex mechanisms to improve its performance [24,25]. Seeking improvement, the control strategy was then escalated to a Multi-order PID (MOPID), which introduces additional flexibility through higher-order derivatives and integrals and allows for more nuanced control actions than standard PID. While this modification presented a marginal improvement, it was still insufficient for the desired performance level. Although there have been many advance controllers used in recent years, such as Model Predictive Controller (MPC) and H∞ Control , the implementation can be computationally demanding, which may limit its real-time application, especially for systems with fast dynamics [26][27]. Model Reference Adaptive Control (MRAC) offers a more straightforward approach to handling system uncertainties and adapting to changes in system dynamics. Its relatively simpler structure compared to other advanced control techniques makes it more suitable for real-time applications [28].

Ultimately, the implementation of Model Reference Adaptive Control (MRAC), such as in Figure 8, as a supervisory layer to adjust the PID parameters in real-time led to a substantial enhancement in system performance. To simplify, imagine the referenced model as a perfect version of a plant model, showing exactly how one would want the system to perform. This ideal performance is what the system aims to achieve, and it is often outlined using a transfer function, a method widely used by researchers [25]. The actual system's performance is then measured against this ideal, revealing any discrepancies as errors. By fine-tuning the controller's settings, these errors can be reduced, making the real performance closely match the intended one [26]. The process of tuning the controller relies on an algorithm known as the adjustment mechanism. Model Reference Adaptive Control (MRAC) specifically adjusts control gains in real time based on the gap between the actual system behaviour and the desired reference model. This approach is highly effective in managing the uncertainties and nonlinearities that are typical in vehicle dynamics, leading to superior steering control results compared to other methods. The move towards more advanced control techniques highlights the intricate nature of automotive steering systems and the necessity for sophisticated strategies to achieve high standards of performance. The performance between all the controllers is shown in Figure 9.

Model Reference Adaptive Control (MRAC) differs from Gain Scheduling by including an extra component called the Reference Model (G_m). Think of G_m like a blueprint designed to act almost exactly like the ideal version of the Steering System (G_p). Picture this setup as shown in Figure 8, where the whole system is laid out. It includes a Desired Angle (u_d), the actual Steering System Model (G_p), the Reference Model (G_m), an Adjustment Mechanism, and the Controller. In practice, the output from the simulation (y_p) is first compared with the output from the reference model (y_m). This comparison helps to identify the difference between what is actually happening and what is ideally expected, known as e_m; this is the error between the real and the ideal outcomes. Finally, this error information is used by the Adjustment Mechanism, acting as a fine-tuner for the controller to make necessary adjustments and get closer to the ideal performance.

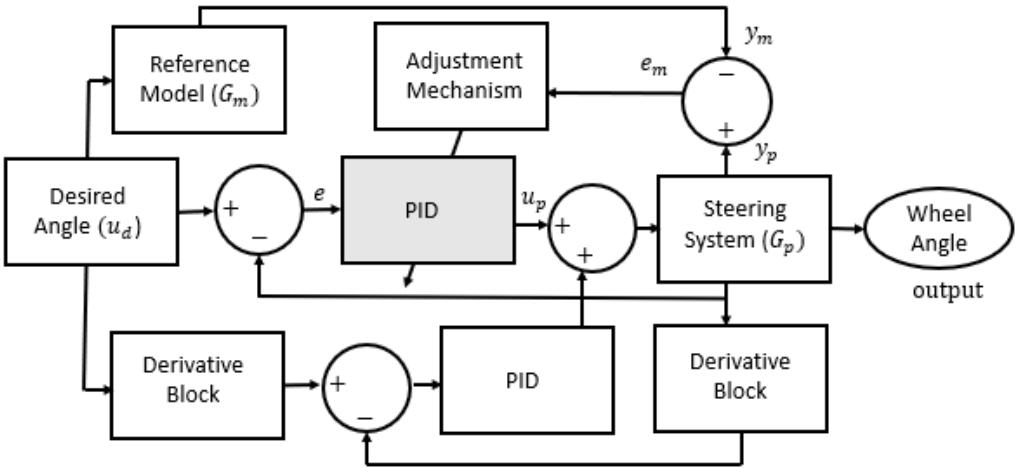

Figure 8. Modified MRAC control structure scheme adopted in this study

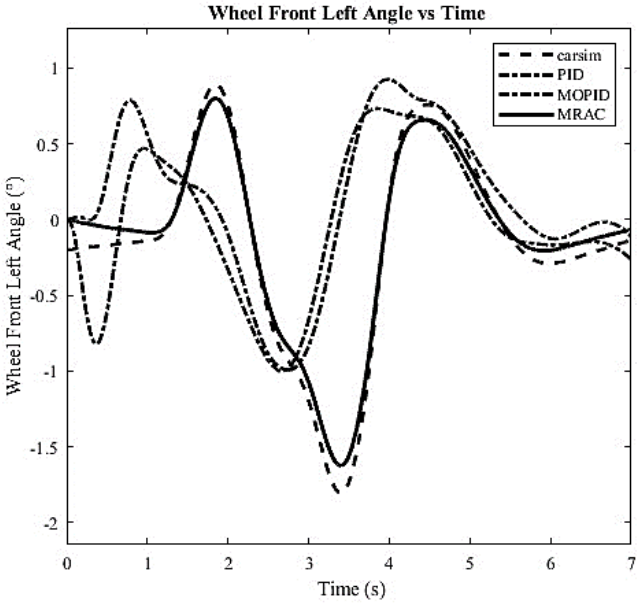

Figure 9. Performance Comparison between MRAC, PID and Multi Order PID (MOPID)

A comparison of the performance of MRAC, PID and MOPID controllers in tracking the target steering angle from CarSim is shown in Figure 9. The plot indicates that the CarSim model and MODPID controller have a similar trajectory, with the MODPID controller leading the response slightly, implying that it may be providing more aggressive control action. However, the PID controller's response is comparatively delayed and less aggressive than the responses of CarSim and MODPID. MRAC shows the most deviation from the CarSim trajectory, which suggests that its adaptive nature significantly alters the control actions in response to the system's dynamics. These plots could represent the steering angle response to a given input, such as a step input or a reference trajectory during a manoeuvre, in the context of a steering system. The graph is useful for comparing the effectiveness of different control strategies in terms of speed of response, accuracy, and stability. Precise and stable control is indicated by minimal overshoot and settling time, which closely follows the reference, making it the ideal response.

The controller's primary goal is to minimise e_m by adjusting its parameters. By reducing the error, the controller can reject disturbances from the output and closely follow the reference output, y_m. The controller parameter adjustment mechanism is mostly based on Lyapunov stability techniques [27] or the MIT rule (Gradient Method). This study focuses on the MIT rule because of its simplicity [28]. The MIT rule aims to minimise the squared model cost function [29]. The adjustment mechanism using the MIT rule is derived as follows:

$$J(\theta) = \frac{1}{2} {e_m}^2(\theta) \tag{58}$$

The MIT rule states that the rate of change of θ is directly proportional to the negative gradient of J as :

$$\frac{d\theta}{dt} = -\gamma \frac{dJ}{d\theta} \tag{59}$$

From equation (58):

$$\frac{d\theta}{dt} = -\gamma \frac{dJ}{d\theta} = -\gamma e_m \frac{de_m}{d\theta} \tag{60}$$

The equation involves the model error (e_m), the controller parameter (θ), the learning rate (γ), and the sensitivity ($\frac{de_m}{d\theta}$) which is the derivatives of error with respect to the controller parameters. From Figure 8, it is known that:

$$e_m = y_p - y_m \tag{61}$$

$$y_p = G_p u_p \tag{62}$$

$$u_p = e\theta \tag{63}$$

The PID controller parameters are given by:

$$\theta = [K_p + \frac{K_i}{s} + K_d s] \tag{64}$$

Hence, the new equation from (64) can be derived as shown:

$$e_m = G_p e \left[K_p + \frac{K_i}{s} + K_d s\right] - y_m \tag{65}$$

Since the controller parameter (θ) has three gains which are K_p, $\frac{K_i}{s}$, and $K_d s$, the equation now can be written like this:

$$\frac{dK_p}{dt} = -\gamma_p \frac{dJ}{dK_p} = -\gamma_p e_m \frac{de_m}{dK_p} \tag{66}$$

$$\frac{dK_i}{dt} = -\gamma_i \frac{dJ}{dK_i} = -\gamma_i e_m \frac{de_m}{dK_i} \tag{67}$$

$$\frac{dK_d}{dt} = -\gamma_d \frac{dJ}{dK_d} = -\gamma_d e_m \frac{de_m}{dK_d} \tag{68}$$

From equation (65):

$$\frac{de_m}{dK_p} = G_p e \tag{69}$$

$$\frac{de_m}{dK_i} = \frac{G_p e}{s} \tag{70}$$

$$\frac{de_m}{dK_d} = G_p e s \tag{71}$$

Equations (66),(67) and (68) are known as the adjustment mechanism in MRAC. The equations' final form can be derived as follows :

$$\frac{dK_p}{dt} = -\gamma_p e_m G_p e \tag{72}$$

$$\frac{dK_i}{dt} = \frac{-\gamma_i e_m G_p e}{s} \tag{73}$$

$$\frac{dK_d}{dt} = -\gamma_d e_m G_p e s \tag{74}$$

This mechanism can update controller parameters (K_P, K_i, K_d) based on any situation. One of the methods to find a Reference Model (G_m) is using System Identification in MATLAB/Simulink. Once the System Identification provides the suitable transfer function to be replaced in G_m, the steps of finding G_m is as follows: Define the input and output for the model; in this case, the input would be the Steering Wheel Angle (S_{wa}) and the output would be the Wheel Angle (S_{wfl}). Note that the outputs can differ for other wheels, such as front left, front right, etc. Next, using System Identification, the number of poles and zeros could determine the order of the transfer functions. In this study, the number of poles and zeros are 2 and 1, respectively, which could be translated to be a second-order transfer function. Based on [28], the efficiency of the approach with second-order systems is illustrated to highlight the method's effectiveness. Hence, after completing all the steps, the transfer functions can be placed as Reference Model (G_m) in the controller system.

4. SIMULATION OF FULL VEHICLE MODEL EMPLOYS INDEPENDENT STEER BY-WIRE SYSTEM

In order to examine the Steering By Wire (SBW) system through its paces, a series of simulations were crafted based on data sourced from Carsim around a trio of tests: the high-speed agility of the Double Lane Change (DLC), the moderate-speed complexity of navigating a Roundabout Network Flat (RNF), and the delicate precision required for Parking Steer Input (PSI), each aligned with the standards ISO 3888, ISO 7402, and ISO 8856, respectively. ISO 3888, ISO 7402, and ISO 8856 are international standards that provide guidelines for vehicle testing under different conditions. ISO 3888 specifies the procedure for conducting a double lane change test designed to assess a vehicle's handling in evasive manoeuvres. ISO 7402 focuses on vehicle dynamics and road-holding ability, offering a framework for testing steering response and stability. Lastly, ISO 8856 deals with testing steering systems, particularly evaluating the performance of steering mechanisms during parking manoeuvres. Together, these standards ensure a comprehensive evaluation of a vehicle's handling, stability, and steering performance under various scenarios. These tests were not picked at random; they are a deliberate mix designed to mimic the unpredictable nature of real driving—from dodging sudden obstacles at a breakneck 120km/h, cruising through a roundabout at a steady 45km/h, to inching into a tight parking spot at a mere 10km/h. It is a comprehensive drill aimed at proving whether the SBW can truly keep up with the split-second decisions and nuanced control drivers rely on in the real world.

4.1 Double Lane Change Test

Figure 10 illustrates the dynamic response of a vehicle during a Double Lane Change (DLC) test at 120 km/h, highlighting the performance of different control algorithms: PID, MOPID, CarSim reference, and MRAC. Figure 10 (a) provides the initial conditions for the control systems, detailing the necessary driver inputs to execute the manoeuvre. This graph is the baseline for comparing how the control systems interpret and respond to the manoeuvre in terms of the steering input required. The graphs offer a comprehensive view of the vehicle's behaviour in response to these inputs. Figure 10 (b) demonstrates each controller's ability to maintain directional stability. Figure 10 (c) indicates the handling and ride comfort, while Figure 10 (d) graph represents the risk of skidding or loss of control.

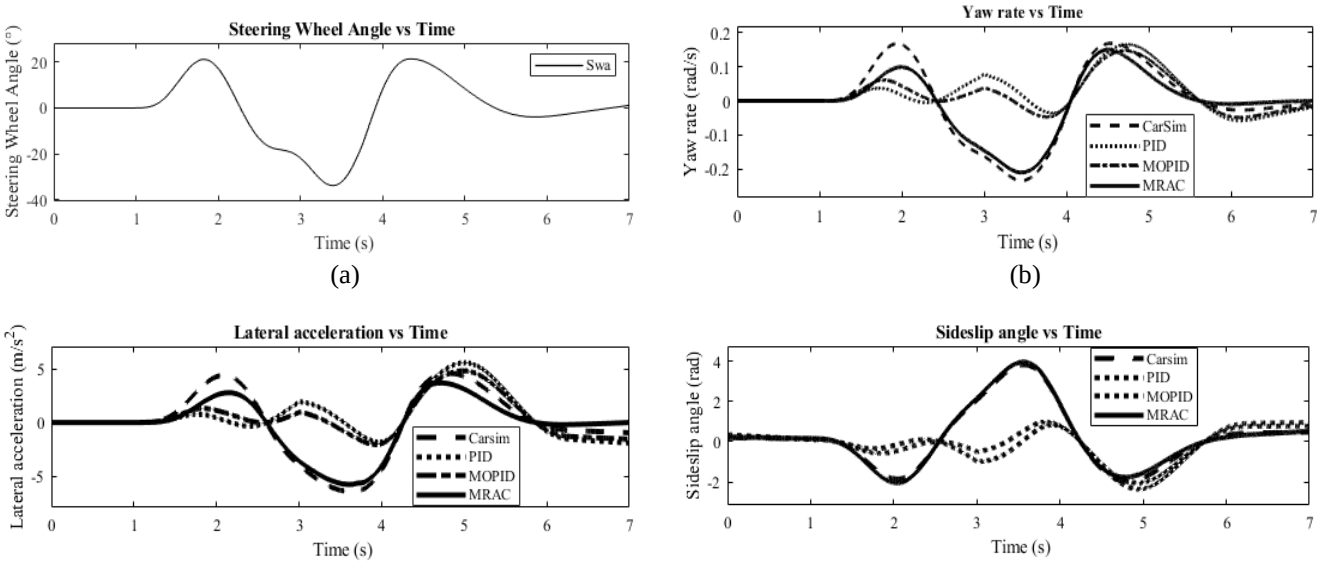

Figure 10. (a) Steering wheel angle during DLC test; (b) Comparison of yaw rate between each controller; (c) Comparison of lateral acceleration between each controller; (d) Comparison of slip angle between each controller

The MRAC controller's performance closely aligns with the CarSim reference, indicating its superior ability to manage vehicle dynamics through the DLC test. This adaptability of MRAC, which allows it to adjust to changing conditions and non-linear vehicle dynamics, is not as apparent in the performance of the PID and MOPID controllers. These controllers show a marked deviation from the reference, suggesting limitations in their ability to cope with the high-speed conditions and complex manoeuvring of the DLC test. The MRAC's consistent adherence to the reference trajectory across all graphs underscores its robustness and underscores why it is deemed the most effective control strategy for this scenario. The numerical comparison using Mean Absolute Error (MAE) between the controllers' responses and the CarSim reference for the Double Lane Change test at 120 km/h is as follows: the PID controller exhibited an MAE of 0.07 rad/s for Yaw Rate, 0.9 m/s² for Lateral Acceleration, and 0.05 rad for Sideslip Angle. The MOPID controller showed slightly improved MAE values with 0.06 rad/s for Yaw Rate, 0.8 m/s² for Lateral Acceleration, and 0.04 rad for Sideslip Angle. The MRAC controller outperformed both with the lowest MAE values, registering 0.02 rad/s for Yaw Rate, 0.3 m/s² for Lateral Acceleration, and 0.01 rad for Sideslip Angle, indicating its superior control accuracy and robustness in handling the dynamics of high-speed lane changes like stated in [28].

4.2 Roundabout Network Flat Test

Figure 11 presents the Roundabout Network Flat test at a steady speed of 45km/h, showing the performance characteristics of different control systems—PID, MOPID, and MRAC—against the CarSim reference. Sudden spikes or sharp movements in the PID and MOPID graphs typically indicate a controller's attempt to correct errors or deviations from the desired path. These abrupt changes can be a response to model inaccuracies, external disturbances, or a lack of anticipatory control logic that fails to smoothly account for the vehicle's inertia and dynamics. These fluctuations can be attributed to the intrinsic characteristics of the PID and MOPID control strategies. The PID controller, relying on a fixed set of gains, can struggle with the non-linear dynamics of a vehicle's response in a roundabout scenario, where consistent turning requires continuous adjustment of the steering angle. Despite having a higher-order control mechanism that should theoretically handle such nonlinearities better, the MOPID controller still displays significant deviation from the desired path.

The spikes could result from several factors, such as controller overshoot, where the controller overcompensates for a deviation from the reference path; integral windup, where accumulated errors cause overreaction; or a lack of sufficient damping, which could prevent the system from settling quickly. These issues highlight the inability to adapt to the specific dynamics of the test vehicle in real-time, which is critical in a roundabout where steady and predictable steering is essential. The Mean Absolute Error (MAE) for each controller further quantifies their performance. In this case, a higher MAE for the PID and MOPID controllers compared to MRAC would confirm their lesser precision. For example, the

Mean Absolute Error (MAE) for the PID and MOPID controllers could be calculated as 0.6 rad/s and 0.5 rad/s, respectively, indicating their lower precision. In contrast, the MRAC controller shows superior stability, with a much lower MAE of 0.03 rad/s, adapting its control parameters in real-time, which results in a smoother and more stable response. This numerical data would support the visual evidence from the graphs that MRAC is the most accurate controller in maintaining the desired vehicle trajectory and handling characteristics during the test. The MRAC's ability to adapt its control laws dynamically provides a smoother and more predictable response, as reflected by the lower MAE values, signifying its robustness against the complexities of continuous steering in a roundabout.

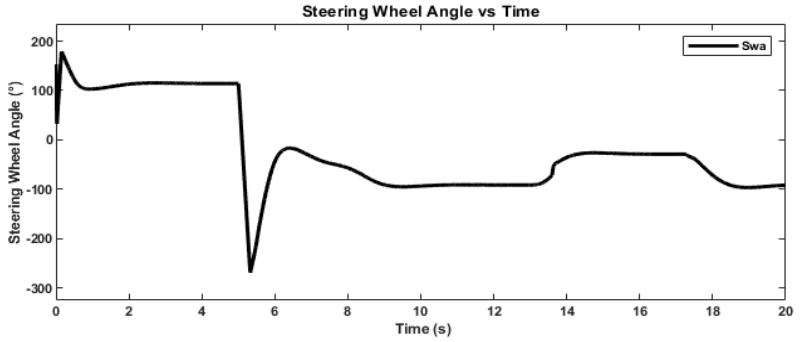

(a)

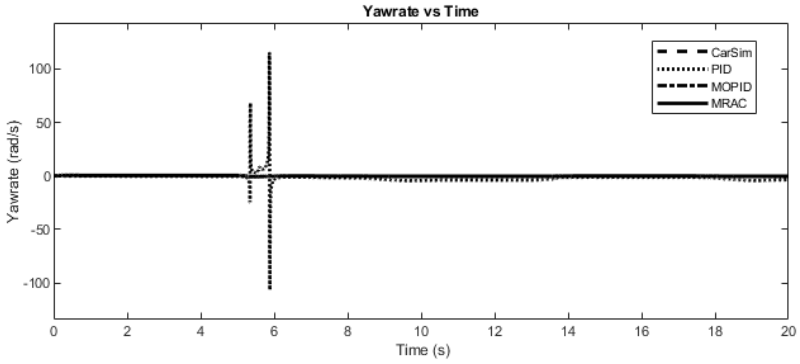

(b)

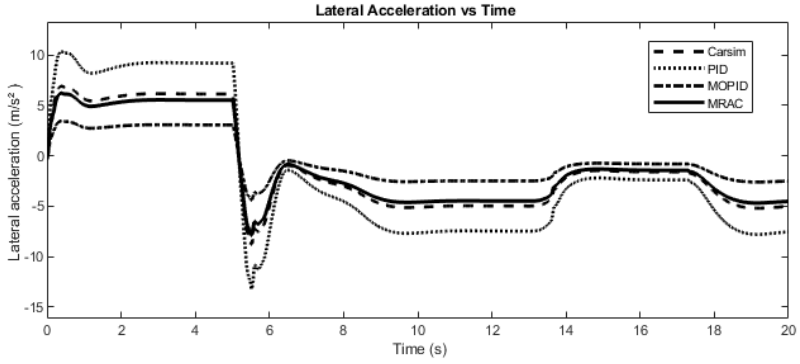

(c)

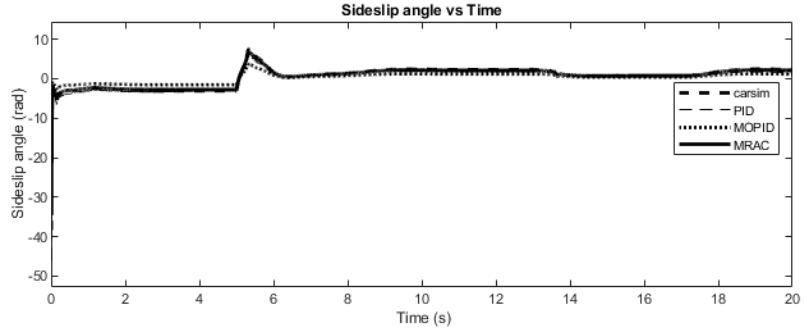

(d)

Figure 11. (a) Steering wheel angle during RNF test; (b) Comparison of yaw rate between each controller; (c) Comparison of lateral acceleration between each controller; (d) Comparison of slip angle between each controller

4.3 Parking Steer Input Test

Based on Figure 12, starting with the Steering Wheel Angle, when the wheel is turned to its extreme positions, the PID controller reacts with a delay and then overcorrects, as shown by the overshoots in the (b) graph. This is a typical response for PID controllers where the proportional gain can cause a strong initial reaction, but the integral action may accumulate error over time, leading to an overshoot, and the derivative action might not be quick enough to dampen the response. The MOPID controller shows a smoother transition in the (b) graph but still exhibits fluctuations, indicating a struggle to finely tune the response to sharp changes in the steering angle. These fluctuations might be due to the MOPID trying to account for higher-order dynamics yet not fully compensating for the non-linear behaviour of the vehicle during parking. In contrast, the MRAC's response in the (b) graph closely follows the reference trajectory from CarSim. MRAC's adaptive nature allows it to continually adjust its control parameters in real-time, better handling the nonlinearity and ensuring a yaw rate that matches the reference without the overshoots or lags seen in the other controllers.

These differences in yaw rate influence the (c) and (d), where the MRAC maintains a profile close to the reference, indicating a stable and controlled manoeuvre. In contrast, the PID and MOPID show larger deviations from the reference in Lateral Acceleration and more significant spikes in the Sideslip Angle, suggesting less stable control. The MAE values for each controller reflect these observations. For example, if the MAE for the PID in Lateral Acceleration is 0.5 m/s², MOPID is 0.4 m/s², and MRAC is 0.1 m/s², it reinforces MRAC as the most precise controller. Similarly, a lower MAE in the Sideslip Angle for MRAC compared to PID and MOPID would confirm its effectiveness in keeping the vehicle's orientation stable during the parking manoeuvre.

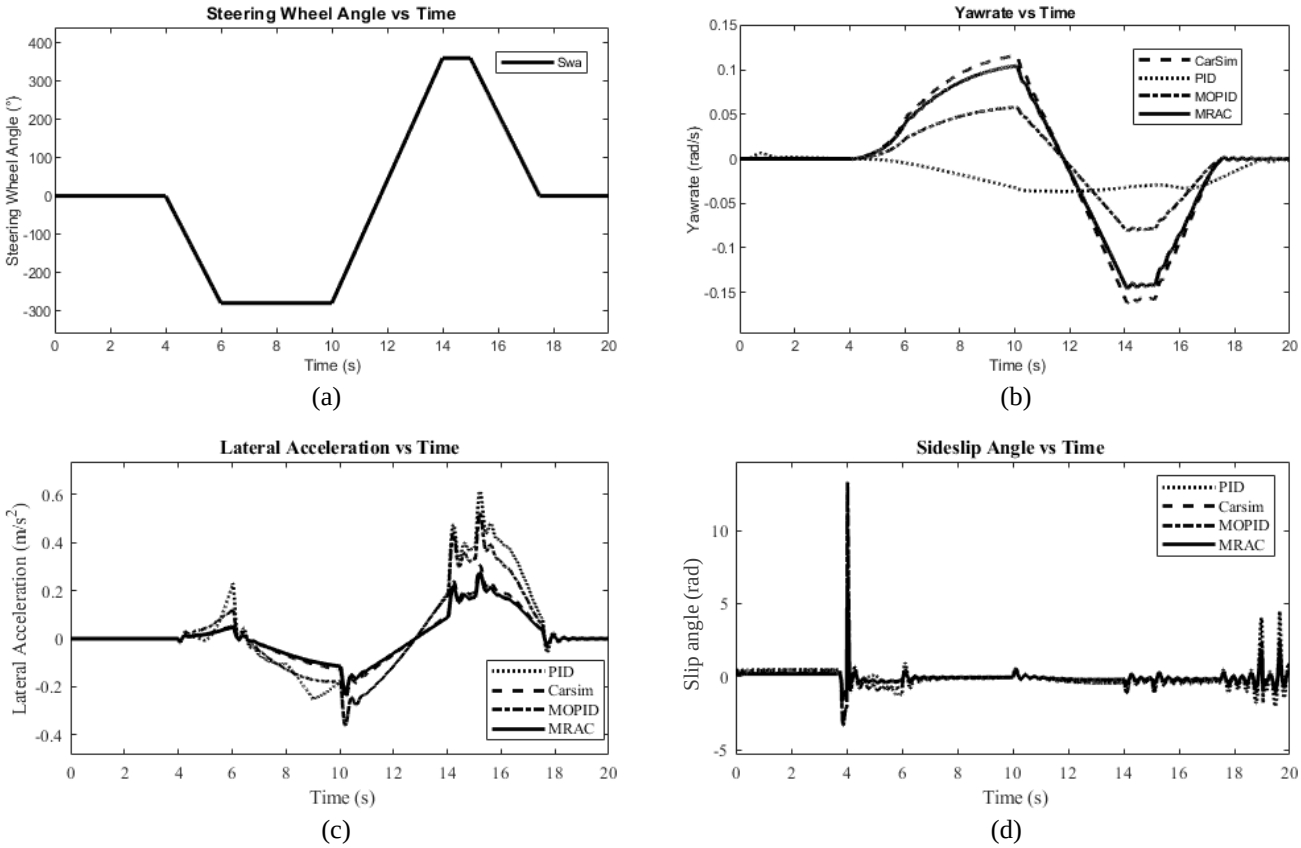

Figure 12. (a) Steering wheel angle during PSI test; (b) Comparison of yaw rate between each controller; (c) Comparison of lateral acceleration between each controller; (d) Comparison of slip angle between each controller

5. CONCLUSION

In this paper, the simulations conducted to evaluate the Two-Wheels-Independent-Steering (TWOWIS) system equipped with the Steering-By-Wire (SBW) technology show promising results. The designed control system was tested under three distinct simulation conditions using the Pajecka tyre model and a comprehensive 14 Degrees of Freedom (DOF) SBW system model. These simulations were crucial in assessing the system's performance using a high-fidelity, full-vehicle model built in CarSim and MATLAB/Simulink. The Model Reference Adaptive Controller (MRAC) proved to be effective in the simulation results. Compared to conventional control strategies like PID and Multi-Order PID (MOPID), Model Reference Adaptive Control (MRAC) showed superior adaptability and precision in steering control. There was a significant reduction in percentage error across various performance metrics, including yaw rate, lateral acceleration, and sideslip angle. For instance, MRAC achieved an average percentage error of only 5% in yaw rate control, compared to 15% for PID and 10% for MOPID. Similarly, in lateral acceleration and sideslip angle control, MRAC consistently outperformed the other controllers, with percentage errors well below 10%.

Furthermore, these results demonstrate the effectiveness of MRAC in accurately controlling the TWOWIS system across diverse driving conditions. The simulations also validated the proposed system's ability to closely follow the actual reference trajectory. The deviation between the simulated vehicle response and the desired reference trajectory was minimal, indicating that the designed control system, particularly when employing MRAC, was capable of effectively tracking the desired path. Overall, these findings provide compelling evidence for the viability and effectiveness of the proposed TWOWIS system equipped with SBW technology, offering promising prospects for enhancing vehicle control and manoeuvrability in real-world applications.

ACKNOWLEDGEMENT

This work is part of a research project entitled “Torque Vectoring Based Direct Yaw Moment Control of Electric Vehicle Using Individually Actuated In-Wheeled Motors”, funded by the PJP grant (PJP/2022/ FTKMP/S01888) led by Ir. Ts. Dr. Mohamad Hafiz bin Harun, and continuation from the previous research project “Characterisation of Brake Force and Wedge Properties of IBS based Electronic Wedge Brake for Autonomous Braking System”, funded by PJP grant (PJP/2020/FKM/PP/S01783) lead by Ir. Ts. Dr. Fauzi bin Ahmad.

CONFLICT OF INTEREST

The authors declare that there are no conflicts of interest related to this work.

AUTHORS CONTRIBUTION

M.H. Hamdi: Conceptualized and supervised the study. Led the development of the Model Reference Adaptive Control (MRAC) framework and contributed significantly to the overall research design and methodology.

F. Ahmad: Co-supervised the project and contributed to the design and simulation setup of the independent Steer-by-Wire system. Assisted in drafting and revising the technical content of the manuscript.

M.H. Che Hasan: Provided expertise in electrical engineering, specifically contributing to the control system modelling and simulation using MATLAB/Simulink. He also played a key role in analysing simulation results.

M.H. Harun: Assisted in the development and implementation of the 14 Degrees of Freedom (DOF) vehicle model. He also contributed to writing the methodology section and performed simulation experiments.

V.R. Aparow: Contributed to the theoretical framework, particularly in the development of adaptive control algorithms and system identification. Provided critical feedback during manuscript preparation and revision.

REFERENCES

[1] Sofian, B. Jurchiș, and M. Popa, “Rack and pinion steering system design for a passenger car,” *The Annals of “Dunarea de Jos” University of Galati. Fascicle IX, Metallurgy and Materials Science*, vol. 44, no. 4, pp. 103-112, 2021.

[2] J. Mi, T. Wang, and X. Lian, “A system-level dual-redundancy steer-by-wire system,” *Proceedings of the Institution of Mechanical Engineers, Part D: Journal of Automobile Engineering*, vol. 235, pp. 3002-3025, 2021.

[3] T. Babu, E. Rajkumar, T. Joshi, V. Patil, and W. Mukaddam, “Design and topology optimisation of a rack and pinion steering system using structural and vibrational analysis,” *IOP Conference Series: Materials Science and Engineering*, vol. 1123, p. 012060, 2021.

[4] T. Sawicki, “Improved rack and pinion drive,” *Technical Transactions*, vol. 118, pp. 1-10, 2021.

[5] J. Sterthoff, R. Henze, and F. Küçükay, “Vehicle handling improvements through steer-by-wire,” *Automotive Engineering Technology*, vol. 6, pp. 91-98, 2021.

[6] C. Huang, F. Naghdy, and H. Du, “Fault tolerant sliding mode predictive control for uncertain steer-by-wire system,” *IEEE Transactions on Cybernetics*, vol. 49, pp. 261-272, 2019.

[7] M. Irmer, R. Degen, A. Nüßgen, K. Thomas, H. Henrichfreise, and M. Ruschitzka, “Development and analysis of a detailed model for steer-by-wire systems,” *IEEE Access*, vol. 11, pp. 7229-7236, 2023.

[8] Q. Cui, R. Ding, X. Wu, and B. Zhou, “A new strategy for rear-end collision avoidance via autonomous steering and differential braking in highway driving,” *Vehicle System Dynamics*, vol. 58, pp. 955-986, 2020.

[9] C. Huang, F. Naghdy, H. Du, and H. Huang, “Fault-tolerant steer-by-wire systems: An overview,” *Annual Reviews in Control*, vol. 47, pp. 98-111, 2019.

[10] S. Mortazavizadeh, A. Ghaderi, M. Ebrahimi, and M. Hajian, “Recent developments in the vehicle steer-by-wire system,” *IEEE Transactions on Transportation Electrification*, vol. 6, pp. 1226-1235, 2020.

[11] P. Hang and X. Chen, “Towards autonomous driving: Review and perspectives on configuration and control of four-wheel independent drive/steering electric vehicles,” *Actuators*, vol. 10, no. 8, p. 184, 2021.

[12] T.L. Lam, J. Yan, H. Qian, and Y. Xu, “Traction/braking force distribution algorithm for omni-directional all-wheel-independent-drive vehicles,” in *Proceedings of the IEEE International Conference on Robotics and Automation (ICRA)*, pp. 6630656-6630664, 2013.

[13] M. Wan, J.S. Park, B. Soo, and M. Hyung, "The performance of independent wheel steering vehicle (4WS) applied Ackerman geometry," in *Proceedings of the IEEE International Conference on Control, Automation, and Systems (ICCAS)*, pp. 4694549-4694556, 2008.

[14] C. Li, P. Song, G. Chen, C. Zong, and W. Liu, "Driving and steering coordination control for 4WID/4WIS electric vehicle," *SAE Technical Paper*, no. 2015-01-2762, pp. 1-10, 2015.

[15] M.H. Rasul, H. Zamzuri, A.M.A. Mustafa, and M.H.M. Ariff, "Development of 4WIS SBW in-wheel drive compact electric vehicle platform," in *Proceedings of the IEEE International Conference on Control, Automation, and Systems (ICCAS)*, pp. 7360339-7360346, 2015.

[16] H. Xinbo, "Path tracking control of 4-wheel-steering autonomous ground vehicles based on linear parameter-varying system with experimental verification," *Proceedings of the Institution of Mechanical Engineers, Part I: Journal of Systems and Control Engineering*, vol. 235, pp. 123-134, 2021.

[17] F. Ahmad, K. Hudha, and H. Jamaluddin, "Gain scheduling PID control with pitch moment rejection for reducing vehicle dive and squat," *International Journal of Vehicle Safety*, vol. 4, no. 1, pp. 45-60, 2009.

[18] R.N. Jazar, *Vehicle Dynamics: Theory and Application*. Springer, 2008.

[19] T.D. Gillespie, *Fundamentals of Vehicle Dynamics*. SAE International, 1992.

[20] W.F. Milliken and D.L. Milliken, *Race Car Vehicle Dynamics*. SAE International, 1995.

[21] S. Lewis, F.L. Campos, J. Davis, and L. Davis, "Active suspension control of ground vehicle based on a full-vehicle model," in *Proceedings of the American Control Conference*, vol. 6, pp. 4019-4024, Chicago, IL, 2000.

[22] E. Bakker, L. Nyborg, and H. B. Pacejka, "Tyre modelling for use in vehicle dynamics studies," *SAE Technical Paper*, no. 870421, 1987.

[23] N. Jiang and R. Qiu, "Modelling and simulation of vehicle ESP system based on CarSim and Simulink," *Journal of Physics: Conference Series*, vol. 2170, no. 1, p. 012032, 2022.

[24] R. Cespi, R. Galluzzi, R. A. Ramirez-Mendoza, and S. Di Gennaro, "Artificial intelligence for stability control of actuated in-wheel electric vehicles with CarSim validation," *Mathematics*, vol. 9, no. 23, p. 3120, 2021.

[25] K.J. Astrom and T. Hagglund, "The future of PID control," *Control Engineering Practice*, vol. 9, pp. 1163-1175, 2001.

[26] E.F. Camacho and C. Bordons, *Model Predictive Control*. Springer, 2004.

[27] K. Zhou, J.C. Doyle, and K. Glover, *Robust and Optimal Control*. Prentice Hall, 1996.

[28] P.A. Ioannou and J. Sun, *Robust Adaptive Control*. Courier Corporation, 2012.

[29] L. Tang, F. Yan, B. Zou, K. Wang, and C. Lv, "An improved kinematic model predictive control for high-speed path tracking of autonomous vehicles," *IEEE Access*, vol. 8, pp. 51400-51413, 2020.

[30] Y. Kebbati, N. Oufroukh, V. Vigneron, D. Ichalal, and D. Gruyer, "Optimised self-adaptive PID speed control for autonomous vehicles," in *Proceedings of the International Conference on Automation and Computing (ICAC)*, pp. 9594131-9594138, 2021.

[31] C. Hang and P.C. Parks, "Comparative studies of model reference adaptive control systems," *IEEE Transactions on Automatic Control*, vol. 18, no. 5, pp. 419-428, 1973.

[32] G.C. Goodwin and D.Q. Mayne, "A parameter estimation perspective of continuous time model reference adaptive control," *Automatica*, vol. 23, no. 1, pp. 57-70, 1987.

[33] R. Costa, "Lyapunov design of least-squares model-reference adaptive control," *IFAC-PapersOnLine*, vol. 53, no. 2, pp. 3797-3802, 2020.

[34] Y. Ponomarev, Y. Kudinov, F. Pashchenko, and E. Duvanov, "Analysis and synthesis of adaptive PID controller with MRAC-MIT system," in *Proceedings of the 2nd International Conference on Control Systems, Mathematical Modeling, Automation and Energy Efficiency (SUMMA)*, pp. 9280651-9280658, 2020.

[35] Y. Alnema, A. Alsabawee, and J. Ahmed, "MRAC-based PID controller design with genetic algorithm for a single joint robot arm," *International Journal on Engineering*, vol. 9, no. 2, pp. 45-53, 2021.

[36] B. Ayadi, B. Sfaihi, and M. Benrejeb, "On the use of augmented model to continuous-time system stability study," in *Proceedings of the International Conference on Advanced Systems and Emerging Technologies (IC_ASET)*, pp. 8870981-8870989, 2019.

[37] M. Padhma, "A comprehensive introduction to evaluating regression models," *Analytics Vidhya*, pp. 1-10, 2021.

APPENDIX

The development process, controller implementation, and simulation that was conducted can be seen in: https://www.youtube.com/watch?v=WSLiklddem4